



Research Article

Development of eco-friendly self-compacting concrete using marble powder, blast furnace slag and glass fibre-reinforced plastic waste: Application of mixture design approach

Manel Djeddou^{*1,a}, Mohamed Amieur^{1,b}, Rabah Chaid^{2,c}, Habib-Abdelhak Mesbah^{3,d}

¹LTPiTE Laboratory, Ecole Nationale Supérieure des Travaux Publics-Francis Jeanson, Kouba, Algeria

²Research Unit: Materials, Processes and Environment, M'hamed Bougarra University of Boumerdes, Algeria

³INSA de Rennes, Université de Rennes 1, L.G.C.G.M. Laboratory, Rennes, France

Article Info

Abstract

Article history:

Received 08 Feb 2024

Accepted 05 May 2024

Keywords:

Marble;

Slag;

Plastic;

Glass;

Fibre;

Concrete;

Mixture design

The present paper investigates the valorisation of three local Algerian waste materials, namely Marble Powder (MP), Ground Granulated Blast Furnace Slag (GGBS), and Glass Fibre-Reinforced Plastic Waste (GFRPW), as mineral additions in Self-Compacting Concrete (SCC). A mixture design modeling approach was used to evaluate the impact of these waste materials and their interactions on the fresh and hardened properties of SCC. Experimental tests were performed, including slump flow, V-funnel, L-box, air content, and compressive strength tests. Regression models were developed to understand the behaviour of SCC based on the proportions of MP, GGBS, and GFRPW in both binary and ternary systems. The statistical analysis software Minitab was employed for the modeling. The results revealed that the combination of MP, GGBS and GFRPW in ternary systems has a synergistic effect on slump flow and L-box ratio. The highest slump flow value and L-box ratio were achieved at proportions of approximately 38% MP, 37% GGBS, and 25% GFRPW. The V-funnel time was affected by the proportions of the waste materials, decreasing with higher MP and GFRPW proportions and increasing with a higher GGBS proportion. In GFRPW-based systems, a higher GFRPW proportion increased the air content, but combining GFRPW with GGBS significantly reduced it. Furthermore, the interaction between GGBS and GFRPW enhanced the development of the 28-day compressive strength, where the highest value of 54 MPa was reached at the combination of 32% GFRPW and 68% GGBS. After 90 days of curing, the SCC mixtures containing 100% GGBS exhibited the highest compressive strength value of 66 MPa. This study provides valuable insights for optimising the use of MP, GGBS, and GFRPW in SCC, potentially leading to more sustainable and cost-effective concrete production.

© 2024 MIM Research Group. All rights reserved.

1. Introduction

Self-compacting concrete (SCC) is a modern form of concrete developed in Japan in 1988 to improve the durability of concrete structures. It was a response to the durability problems that had arisen two decades after post-war reconstruction, where the focus on rapid project delivery had compromised the quality of construction (1). Prof. Hajime Okamura identified insufficient concrete compaction as a major cause of structural deterioration and proposed SCC as a solution (1). This new technology allows concrete to be placed into the formwork under its own weight without the need for vibration. As well as improving the durability of concrete structures, SCC has helped to address the shortage of skilled labour in the construction industry. The SCC mix design necessitates a high

*Corresponding author: m.djeddou@enstp.edu.dz

^a orcid.org/0009-0002-5007-9944; ^b orcid.org/0000-0002-6650-942X; ^c orcid.org/0000-0002-7008-4161;

^d orcid.org/0000-0003-1705-4681

DOI: <http://dx.doi.org/10.17515/resm2024.178ma0208rs>

Res. Eng. Struct. Mat. Vol. x Iss. x (xxxx)xx-xx

cement content with a compatible rate of superplasticizer. This composition is essential for the concrete to achieve fresh properties, including segregation resistance, filling ability, and passing ability, that characterise SCC and contribute to its self-place ability. However, the adoption of this technology in the construction industry can increase the cost of concrete production and its carbon footprint (2). Many researchers have proposed the use of industrial by-products such as marble dust, granulated blast furnace slag, and glass fibre-reinforced plastic waste, as mineral additions in SCC. This approach offers several benefits, such as material cost reduction, decreased environmental impact, and enhanced concrete performance.

Marble is a metamorphic rock composed mainly of carbonate minerals such as dolomite and calcite. Valued for its durability, resistance, and wide range of colours, it has long been used as a building material and decorative element. The extensive global production of this stone has resulted in negative impacts on the environment and public health. Dust generated during the processing, cutting, and polishing of marble is collected and discharged near the manufacturing plants. The high alkalinity of these deposits reduces soil fertility and increases the risk of water contamination (3,4). In addition, the fine marble particles suspended in the air can cause respiratory, visual, and skin disorders (5), (6). To mitigate the environmental impact of MP, numerous researchers have attempted to use this waste material in the production of SCC. Meera et al. (7) analyzed the rheological and mechanical behavior of SCC containing up to 360 kg/m³ of MP. Most of the mixes were classified within the VS2/VF1 and VS2/VF2 categories of the EFNARC specifications. The authors concluded that MP can be used in low-strength SCC up to 360 kg/m³ and in high-strength SCC up to 230 kg/m³. Gupta et al. (2) conducted a study to investigate the use of marble waste (MP), silica fume (SF), and fly ash (FA) in different combinations for the design of high-performance self-compacting concrete (HPSCC). The addition of both MP and FA was found to enhance the fresh properties of HPSCC. The use of 10% MP combined with 15% FA and 5% SF exhibited the best mechanical performance and microstructure of HPSCC. Sadeek et al. (8) highlighted that the incorporation of MP without cement substitution enhances the mechanical performance of SCC. Mechanical strength showed an increase with higher incorporation rates of MP. Mahmood et al. (9) concluded that substituting 5% of fine aggregate with marble powder and 15% with rice husk ash resulted in optimum mechanical performance for both short and long-term applications in SCC.

Blast furnace granulated slag is a by-product of iron production that is typically landfilled, causing environmental damage such as soil degradation and water pollution. Ground granulated blast furnace slag (GGBS) is a well-known material that, due to its latent hydraulic reactivity, is widely used as a partial substitute for cement in cement-based materials. Several studies have focused on its use in SCC and reported various results. Bayat et al. (10) found that substituting cement with up to 40% GGBS generates SCC mixes with reduced flowability, viscosity and passing ability. However, the incorporation of GGBS at 30% cement replacement optimized mechanical strength. Sara et al. (11) showed that the addition of GGBS as a cement substitute in self-compacting mortar based on recycled concrete sand reduced the demand for superplasticizers. The highest compressive strength was achieved at a cement substitution rate of 20%. By investigating the behaviour of SCC after replacing up to 60% of cement with GGBS, Mohammed et al. (12) reported that the mechanical strength increased, reaching an optimum value of 84 MPa at a substitution rate of 40% and a water/cement ratio of 0.26. According to Ofuyatan et al. (13), the use of GGBS results in a decrease in flowability and an increase in viscosity and passing ability. The SCC mixes exhibited optimum mechanical strength at 20% cement substitution.

Glass Fibre-Reinforced Plastic (GFRP) is a composite material consisting of glass fibres immersed in a thermosetting resin. GFRP is known for its exceptional properties that combine lightness with high mechanical and durability performance. These properties

have facilitated its widespread adoption in various industries, including aerospace, construction, and automotive. The growing global market demand for composite materials has resulted in the accumulation of waste generated during their production, including machining, cutting, and polishing. The GFRP products are also expected to reach the end of their service life, leading to the accumulation of even larger quantities of this material. The accumulation of GFRPW is a significant challenge that requires sustainable waste management and recycling practices. Mechanical recycling is a promising approach for the management of GFRPW, as it is cost-effective and environmentally friendly [14]. This method involves shredding or grinding the waste into small pieces that can then be used as raw materials for new products. Other methods of recycling GFRW, such as chemical and thermal recycling, are also being explored, but are generally more expensive and energy-intensive (16). The incorporation of mechanically recycled GFRP powder in cement-based materials offers a promising solution for waste management in the construction sector, helping to mitigate the negative impact of this waste on the environment. Most studies on the incorporation of recycled GFRP powder as a replacement for fine aggregates in concrete and mortar have reported a loss of workability and a degradation of mechanical strength (17–21). However, recent research has shown that the use of a small amount of recycled GFRPW in cement-based materials can improve their mechanical performance. Asokan et al. discovered that oven curing allows the mechanical strength of GFRP powder-based concrete to develop (20). The same authors, in another study, found a significant improvement in mechanical strength when GFRPW is incorporated with a high dosage of superplasticizer (22). Farinha et al. also reported a continuous increase in the mechanical strength of mortar by substituting natural silica sand with GFRP powder obtained from the cutting process of floor elements (23). Tittareli and Moriconi (24) have used GFRP powder in SCC by replacing the calcareous filler at rates of 25% and 50%. The authors reported a considerable loss in mechanical resistance despite the improvement of some durability-related properties.

The extensive investigation of the potential for recycling MP, GGBS and GFRPW as alternatives to cement or fine aggregates has been the focus of numerous research efforts. These studies have mainly concentrated on the use of these waste materials alone or in combination with other mineral additions such as pozzolan (PZ) (25), fly ash (FA), and silica fume (SF)(2). However, to date, no studies have examined the simultaneous use of these wastes in SCC or other cement-based materials.

The objective of this work is to investigate the effect of combining the three types of waste (MP, GGBS, and GFRPW) in binary and ternary systems on the fresh and hardened properties of SCC. The waste additions were ground to a consistent Blaine fineness of 4500 cm²/g to eliminate the influence of this physical property on the concrete's performance. The fresh properties of SCC were evaluated through a series of tests, including slump flow, V-funnel time, L-box ratio, and air content. Additionally, the mechanical properties were assessed through compression tests after 28 and 90 days of curing. In this study, the mixture design method, a statistical approach, was employed to analyse the individual and combined effects of MP, GGBS, and GFRPW on the properties of the SCC under investigation. This approach provides a comprehensive understanding of the impact of these waste materials on the performance of SCC.

2. Experimental Program

2.1. Mixture Design Approach

The mixture design method is a statistical modelling tool specifically tailored to analyse the behaviour of mixtures (blends). This approach is particularly valuable in construction materials such as concrete, where it enables the design of experiments, prediction of concrete behaviour, and optimisation of the proportion of its components to achieve the

best performance. The mixture plan is an experimental design characterised by a fundamental constraint indicating that the proportion of all the mixture components must add up to 100%. This constraint is expressed in equation (1), where X_i denotes the proportion of the constituent i (26).

$$\sum_{i=1}^{i=n} X_i = 1 \quad (1)$$

The mixture design of experiments is beneficial in understanding the relationship between the behaviour of a mixture, referred to as "response Y," and the proportion of its constituents X_i , termed factors. It is evident that the factors are non-independent, where the proportion of a specific component depends on the combined proportions of the other ingredients. The experimental programme can be defined based on the type of mixture design adopted. The simplex lattice, simplex centroid, and extreme vertex are traditional mixture designs that help determine the number of mixtures to be prepared with the proportions of their analysed constituents. Once the experiments have been conducted on these mixtures, the regression equation can be developed to describe the association between the response Y and the factors X_i . The regression equation provides insights into the impact of each constituent and their interactions on the behaviour of the mixtures. Furthermore, it enables the effective prediction of the mixtures' performance based on the proportions of their constituents. The validity of the regression equation is subsequently assessed using specific parameters, including the coefficients R^2 , R^2_{adj} , and R^2_{pred} , analysis of variance (ANOVA), and the distribution of errors between the experimental and predicted results (residuals) (27). This evaluation process is essential for determining the accuracy and reliability of the regression model in describing the data and making predictions.

$$Y = B_1 \times MP + B_2 \times GGBS + B_3 \times GFRPW + B_4 \times (MP \cdot GGBS) + B_5 \times (MP \cdot GFRPW) + B_6 \times (GGBS \cdot GFRPW) + B_7 \times (MP \cdot GGBS \cdot GFRPW) \quad (2)$$

In this study, a ternary system composed of MP, GGBS, and GFRPW was evaluated for its suitability as a mineral addition in self-compacting concrete. The traditional augmented simplex-centroid mixture plan, based on three factors, was employed, resulting in 10 combinations to be processed, as illustrated in Fig. 1. The special cubic model of Scheffé was selected for the regression equation, which includes the individual factors MP, GGBS, and GFRPW, along with their binary and ternary interactions, as detailed in equation (2). The coefficients of the regression model (B_i) were calculated using the least squares method, which minimises the sum of the squares of the errors. These coefficients represent the contribution of the associated terms to the response variable "Y". A high coefficient indicates a strong influence on the response, while a negative coefficient suggests an adverse influence on the variable "Y". The mixture design approach was applied in this investigation using the Minitab statistical software.

2.2. Materials

The used cement is a blended Portland cement of type CEM II/A-L 52.5 N, manufactured by the CILAS cement plant (Ciment Lafarge Souakri) in accordance with the European Standard EN 197-1 (Fig. 3(a)).

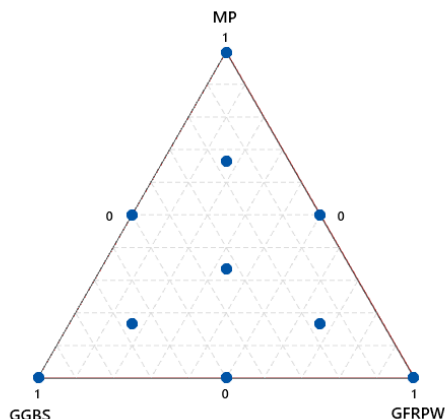


Fig. 1. Illustration of centroid-simplex augmented design with three factors: MP, GGBS and GFRPW

Three Algerian industrial by-products, MP, GGBS, and GFRPW, were utilised as mineral additions in SCC. The MP was obtained from the El-Khroub quarry near the city of Constantine, whilst the GGBS was from the El-Hadjar steel factory in Annaba (Algeria). The GFRPW was recovered from the “Maghreb Pipe Industries” factory located in M’sila (Algeria), which specialises in the production of GFRP piping systems. This waste material is generated as a by-product of the GFRP pipe-cutting process. The cutting equipment includes a vacuum system that collects and stores the GFRP waste in bags (Fig. 2). The GFRP itself was produced using polyester thermosetting resin and E-glass fibres. The chemical composition of cement, MP, GGBS and GFRPW obtained with X-ray fluorescence (XRF) analysis is presented in Table 1.

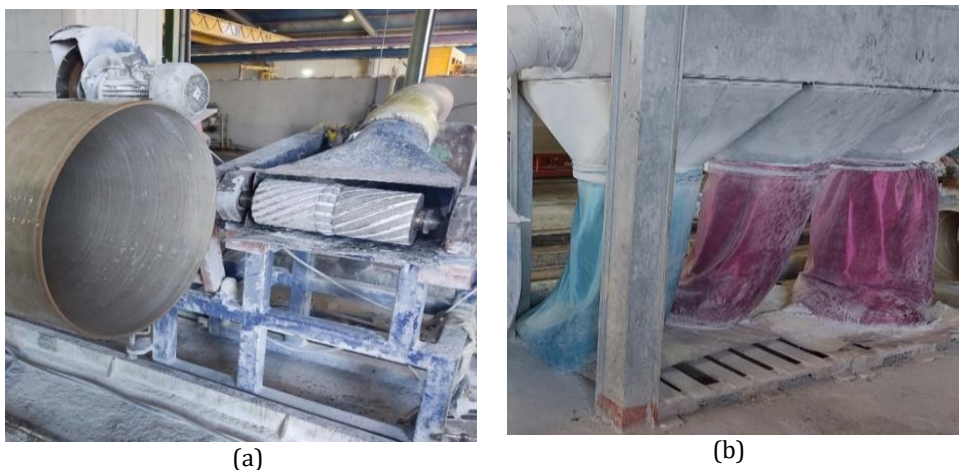


Fig. 2. (a) Cutting process of GFRP pipes with the vacuum system, (b) GFRPW Storage bags

All the waste materials (MP, GGBS, and GFRPW) were ground separately using a ball mill until their Blaine-specific surface area reached $4500 \text{ cm}^2/\text{g}$ (Fig. 3(b), (c), (d)). Scanning electron microscopy (SEM) analysis was conducted to examine the morphology and surface texture of the waste particles after the grinding process. The marble particles were found to possess a relatively rounded shape with a smooth surface (Fig. 4 (a)), whereas the

GGBS consisted of angular particles with a rough surface (Fig. 4 (b)). The GFRPW was characterised by the irregular shape and size of its particles (Fig. 4 (c)). The physical properties and particle size distribution of MP, GGBS, GFRPW, and cement are presented in Table 2 and Fig. 5, respectively.



Fig. 3. (a) General aspect of Cement, (b) MP, (c) GGBS and (d) GFRPW

Table 1. Chemical composition of Cement, MP, GGBS and GFRPW

Materials	SiO ₂	Al ₂ O ₃	Fe ₂ O ₃	CaO	MgO	SO ₃	K ₂ O	Na ₂ O	TiO ₂	LOI
Cement	19.47	4.89	2.97	64.58	1.63	2.28	0.74	0.12	-	2.97
MP	0.06	-	0.01	55.73	0.12	0.07	-	-	0.01	43.65
GGBS	35.65	7.86	4.83	40.87	3.50	1.62	0.63	0.12	0.28	0.02
GFRPW	33.44	8.29	0.24	11.85	1.56	0.08	0.06	0.42	0.25	44.32

Table 2. Physical properties of MP, GGBS, GFRPW and Cement

Materials	MP	GGBS	GFRPW	Cement	Specifications
Specific Gravity	2.72	2.92	1.77	3.09	EN 1097-7
Blaine fineness (m ² /Kg)	450	450	450	390	EN 196-6

Three fractions of crushed natural aggregates were utilised in this work: gravel (3/8), gravel (8/15), and sand (0/4) obtained from the Kef-Azrou quarry located in Medea (Algeria), and dune sand of class (0/1) collected from Bou-Saada in southern Algeria. The physical characteristics and gradation curves of the fine and coarse aggregates are presented in Table 3 and Fig. 6, respectively.

A polycarboxylate-based superplasticizer, Sika ViscoCrete Tempo 12, with a specific density of 1.06 and a solid content of 30%, was used.

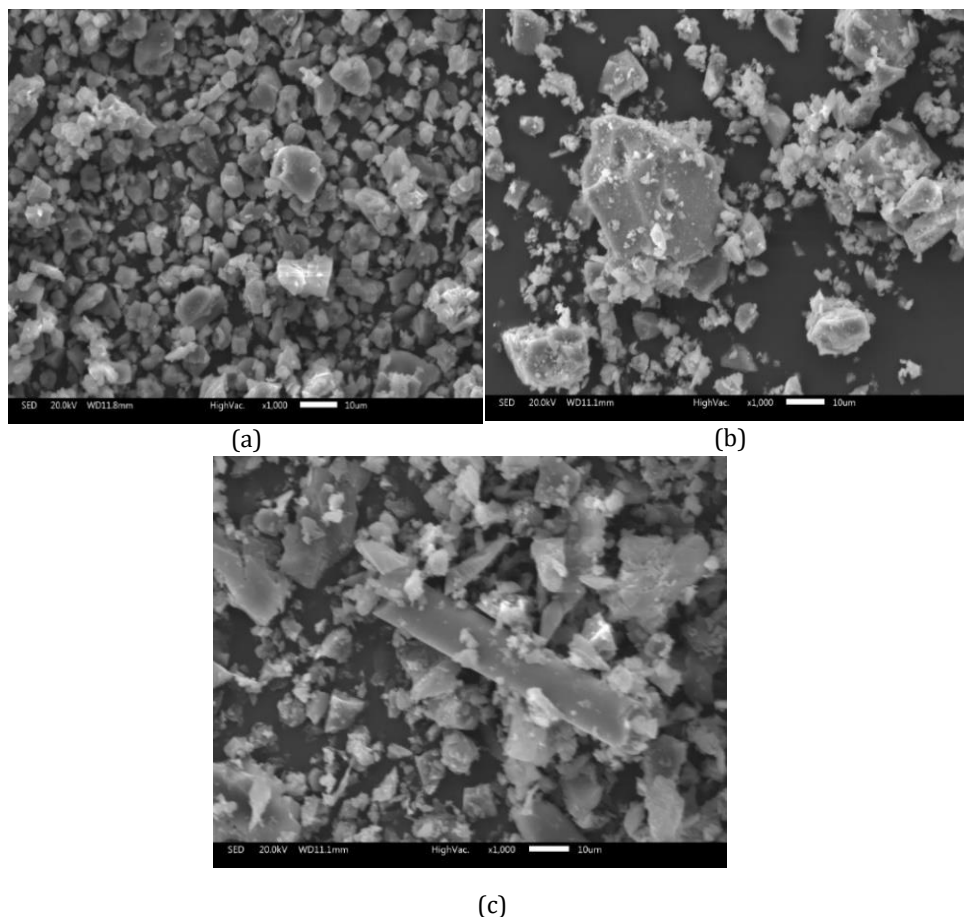


Fig. 4. SEM observation of MP (a), GGBS (b), and GFRPW (c).

Table 3. Physical characteristics of aggregates

Materials	Gravel 1 (8/15)	Gravel 2 (3/8)	Crushed Sand (0/4)	Dune Sand (0/1)	Specifications
Specific Gravity	2.62	2.64	2.74	2.62	EN 1097-6
Coefficient of absorption	1.01	1.19	0.73	0.55	
Flakiness index	11.46	14.37	-	-	EN 933-3
Sand equivalent (%)	-	-	60.78	75.75	EN 933-8
Methylene Blue Value	-	-	0.17	1.83	EN 933-9
Fineness Modulus	5.93	5.24	3.06	1.03	NF P 18-540

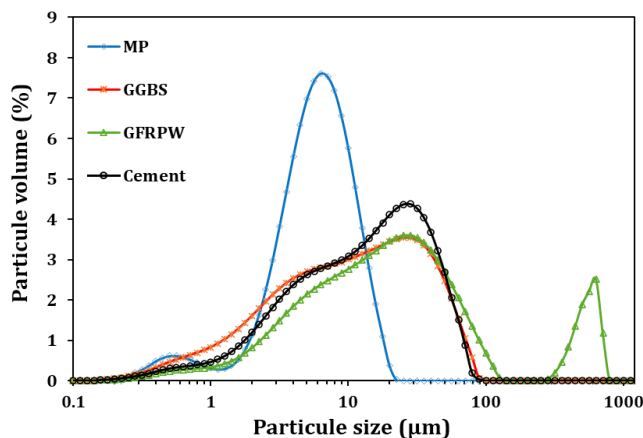


Fig. 5. The gradation curves of MP, GGBS, GFRPW and Cement

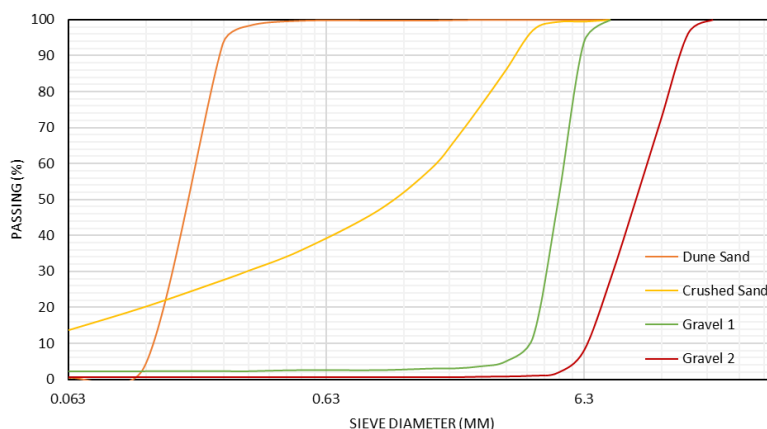


Fig. 6. The gradation curves of Dune sand, crushed sand, gravel 1 and gravel 2.

2.3. Mixture Proportions

This study involves the preparation of 10 mixtures of SCC. The mineral addition, consisting of MP, GGBS, and GFRPW, was incorporated into the SCC mixtures at a proportion of 15% of the cement mass. The proportions of MP, GGBS, and GFRPW were determined according to the mixture design plan, as shown in Table 4. The quantities of the additional components, such as cement, gravel, sand, water and superplasticizer (SP), in the SCC mixture were kept constant, and their specific values are detailed in Table 5.

2.4. Testing Procedure

The experimental evaluation of the SCC mixtures included tests to assess their fresh and hardened properties. The tests conducted to evaluate the fresh properties included the slump flow (EN 12350-8), V-funnel time (EN 12350-9), and L-box (EN 12350-10) tests. The slump flow test was conducted by using a slump cone mould to contain the SCC mixture. The process involved filling the slump cone with the SCC sample without any compaction and lifting it vertically to allow the concrete to flow freely. After lifting the

slump cone, the final diameter of the resulting concrete spread was measured in two directions (Fig. 7(a)). For the V-funnel test, the SCC sample was poured into a V-funnel apparatus until it reached the top. The trap door was then opened, and the time it took for the concrete to flow out was recorded. The L-box test involved the use of an L-shaped box apparatus consisting of a vertical section connected to a horizontal section through a control gate. To perform the L-box test, the SCC sample was initially poured into the vertical section. The control gate was then removed to allow the SCC to flow through the horizontal part. The heights of the concrete at the end (H2) and the beginning (H1) of the L-box horizontal section were measured after the fresh concrete flow ceased (Fig. 7(b)). The blocking ratio was calculated as H2/H1. The air void content of the fresh SCC mixtures was measured using an air meter (ASTM C 231), as shown in Fig. 7(c). SCC specimens were cast in cylindrical moulds measuring ϕ 100 x 200 mm and placed in a controlled chamber at $20 \pm 5^\circ\text{C}$ for 24 hours. Following demoulding, the concrete specimens were immersed in water at $20 \pm 2^\circ\text{C}$. The compressive strength test (EN 12390-3) was carried out on the hardened concrete specimens after 28 and 90 days of water curing, as shown in Fig. 7(d). The results of these tests are detailed in Table 4.

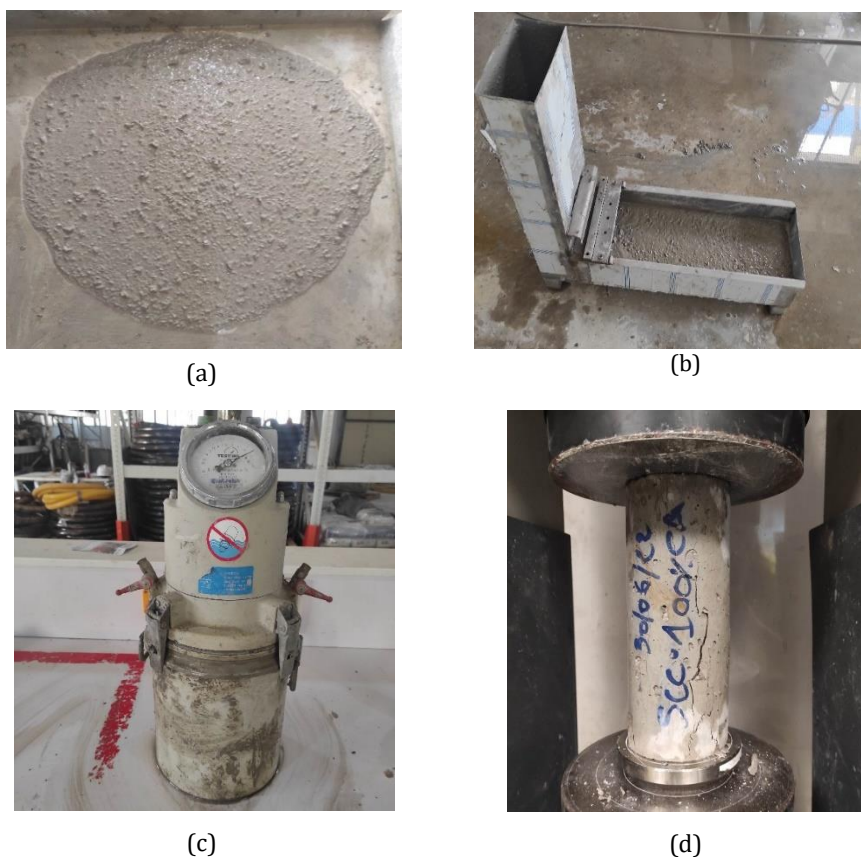


Fig. 7. (a) Tests for SCC: Slump flow, (b) L-box, (c) Air content, (d) Compressive strength

Table 4. Waste materials combinations and experimental results of prepared SCC mixtures.

Mix. N°	Waste materials combinations			Fresh Properties				Compressive strength (MPa)	
	MP	GGBS	GRPW	Slump Flow (mm)	V-funnel time (s)	L-box ratio (H2/H1)	Air Content (%)	Rc28	Rc90
1	1	0	0	695	10	0.87	2.30	49.38	51.99
2	0	1	0	700	23	0.86	3.00	51.02	66.12
3	0	0	1	590	10	0.84	3.90	41.65	48.57
4	1/2	1/2	0	690	14	0.86	2.10	48.72	49.82
5	1/2	0	1/2	615	9	0.80	3.10	44.04	51.69
6	0	1/2	1/2	625	18	0.78	2.30	53.29	61.73
7	1/3	1/3	1/3	720	15	0.92	2.35	49.63	55.54
8	2/3	1/6	1/6	730	12	0.91	2.00	50.67	51.77
9	1/6	2/3	1/6	740	16	0.89	2.10	53.90	59.03
10	1/6	1/6	2/3	650	10	0.85	3.20	45.58	53.72

Table 5. Quantities of SCC mixture constituents kept constant.

Materials	Gravel 1	Gravel 2	Crushed Sand	Dune Sand	Cement	Mineral addition*	Water	SP
Quantity (Kg/m ³)	297	445	868	96	400	60	206	2.76

*(MP+GGBS+GFRPW)

3. Statistical Analysis of Regression Models

The regression models are established to evaluate the effect of MP, GGBS, and GFRPW proportions, and their interactions, on each of the SCC properties investigated. The analysis of variance (ANOVA) is a statistical method that helps to estimate and verify regression models through the P-value that determines the statistical significance of the model terms. A P-value less than 0.05 indicates that the model terms are significant, whilst a P-value greater than 0.05 identifies non-significant terms at a 95% confidence level. The presence of non-significant terms in the regression model can affect its descriptive and predictive quality. This work applies the stepwise elimination method to eliminate non-significant terms from the developed models. In the stepwise regression process, terms are systematically added to or removed from the model based on their statistical significance. Table 6 shows the final form of all established regression models, along with their respective R^2 , R^2_{adj} , and R^2_{pred} coefficients. In regression analysis, the R^2 and R^2_{adj} coefficients are used to evaluate the goodness of fit of the derived model with the experimental results, while the R^2_{pred} coefficient is used to assess the predictive capacity of the model for new observations that deviate from the initial dataset. The validation of the statistical models also involves residual diagnostics, which include analysing the residuals against the predicted responses, as presented in Fig. 8. A random distribution of residuals in these plots indicates that the data does not exhibit any systematic patterns, such as reliability, periodicity, or interference (28). This randomness provides evidence that the model is validated and can be considered appropriate for the given application.

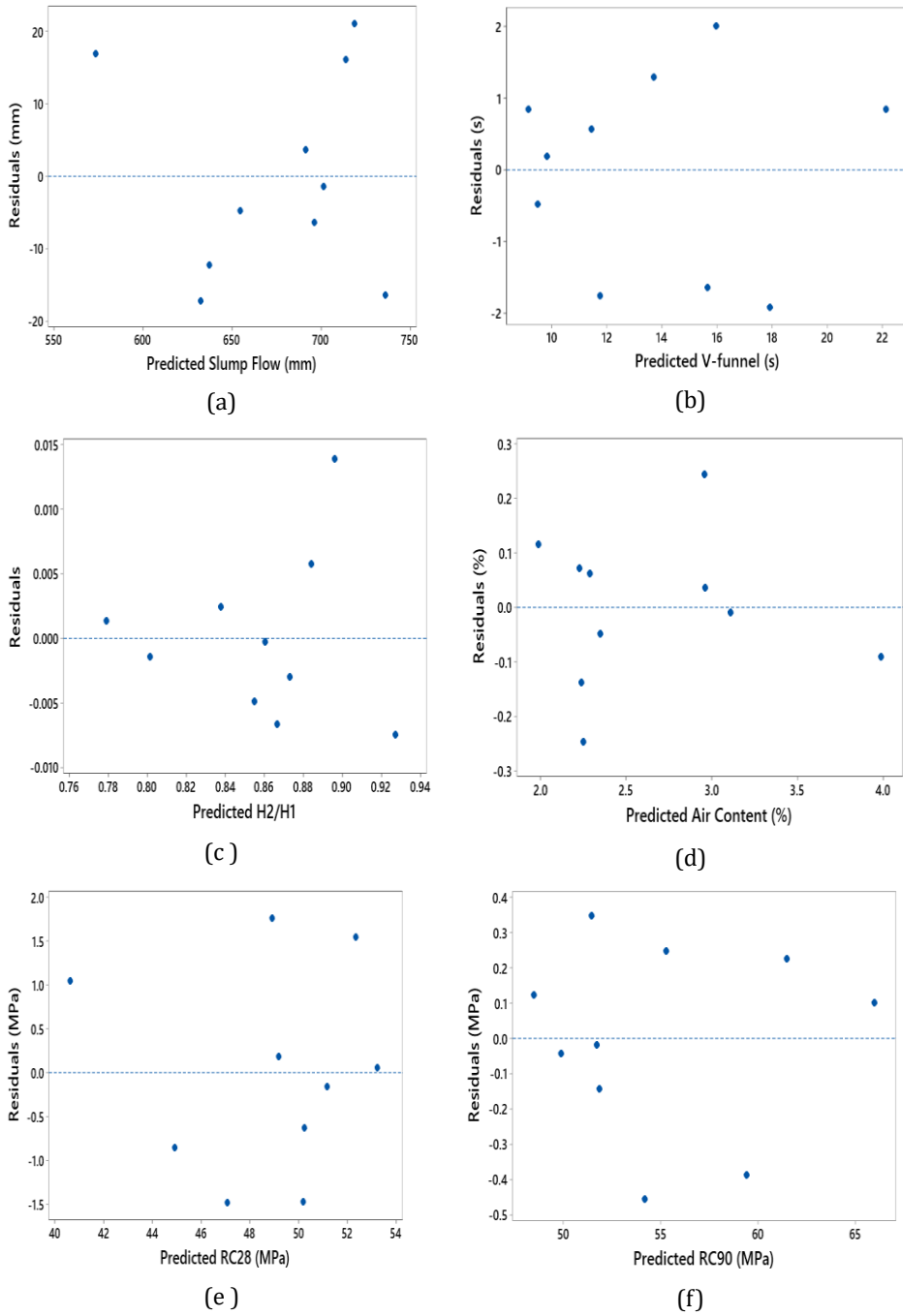


Fig. 8. Residual plots for: (a) Slump flow, (b) V-funnel, (c) H2/H1, (d) Air Content, (e) RC28, (f) RC90.

Table 6. Regression equations developed by the mixture design approach and respective square R.

Response	Equation	R ²	R ² _{adj}	R ² _{pred}
Slump Flow (mm)	$691.3*MP + 701.3*GGBS + 573.0*GFRPW + 2190*MP*GGBS*GFRPW$	92.71	89.06	76.19
V-funnel (s)	$9.14*MP + 22.14*GGBS + 9.81*GFRPW$	90.27	87.49	82.02
H2/H1	$0.873*MP + 0.860*GGBS + 0.837*GFRPW + 3.393*MP*GGBS*GFRPW - 0.281*GGBS*GFRPW - 0.216*MP*GGBS*GFRPW$	97.89	95.26	82.76
Air content (%)	$2.227*MP + 2.963*GGBS + 3.991*GFRPW - 4.517*GGBS*GFRPW - 2.444*MP*GGBS$	95.09	91.16	75.15
Rc28 (MPa)	$49.19*MP + 51.18*GGBS + 40.60*GFRPW + 29.38*GGBS*GFRPW$	91.32	86.97	75.28
Rc90 (MPa)	$51.83*MP + 66.01*GGBS + 48.45*GFRPW - 36.26*MP*GGBS + 17.09*GGBS*GFRPW + 6.28*MP*GFRPW + 34.9*MP*GGBS*GFRPW$	99.78	99.34	92.94

4. Results and Discussion

4.1. Slump Flow

The trace plot established by Minitab helps in understanding the individual effect of each component on the response value (28). According to the response trace plot of slump flow, illustrated in Fig. 9, it can be seen that the three components, MP, GGBS, and GFRPW, have a positive effect in a particular range where the slump flow value increases, followed by a negative effect where the slump flow value decreases. It can also be seen that the MP and GGBS have a similar effect on the slump flow value, which is demonstrated by the superposition of their corresponding curves. This behaviour can be explained by these two components having the same specific surface area. The amount of water required to lubricate the surface of GGBS and MP particles can be the same, making the MP- and GFRPW-based SCC mixes exhibit similar slump flow diameters (23). However, the curve corresponding to GFRPW shows a significant drop in slump flow value, even though its specific surface area is the same as that of MP and GGBS. Correia et al. (19) reported a similar observation, which was attributed to the irregularity and non-uniformity in size and shape of GFRPW particles as compared to the spherical and uniform particles of recycled stone slurry. Oliveira et al. (17) explained the increased water consumption resulting from the incorporation of GFRPW due to the irregular dimensions of its particles, as shown in Fig. 4(c). Zhou et al. (29) also highlighted the effect of GFRPW-particle size distribution on workability. The authors observed that GFRW, consisting of two dominant particle sizes, namely short glass fibres and angular resin particles, negatively affects the workability of mortar. As shown in Fig. 5, the GFRPW used in our study is dominated by two main particle sizes, which may explain the slump flow drop. Furthermore, the presence of cylindrical-shaped particles in GFRPW (Fig. 4(c)) results in a loss of workability and a reduction in slump flow diameter as the proportion of GFRPW increases (30). Hadigheh et al. (14) attributed the decrease in slump flow diameter observed with a higher GFRPW dosage to the conglomeration of fibrous and granular recycles, thus increasing the water demand.

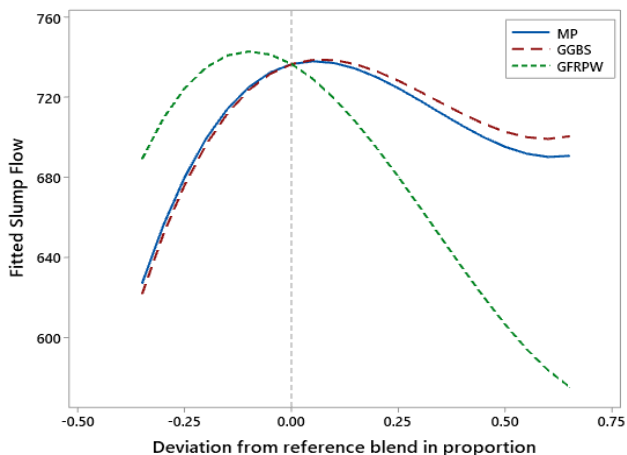


Fig. 9. Trace plot for Slump flow

The statistical model derived for the slump flow (Table 6) indicates that the latter is mainly influenced by the combination factor $MP*GGBS*GFRPW$ in a ternary system (2190). It can be seen that the interaction between the three additions generates a synergistic effect on the slump flow. This effect better elucidates the observed increase in slump flow values shown in Fig. 9. Dada et al. reported similar behaviour in a ternary system combining marble powder, pozzolana, and cement. They explained the decrease in workability that followed the synergistic effect by an increase in the compactness of the mixes (31). The ternary contour plot in Fig. 10 illustrates the effect of MP, GGBS and GFRPW proportions on slump flow in ternary and binary systems. This figure shows that SCC mixes containing more than 0.5 GFRPW proportion in the GFRPW-GGBS and GFRPW-MP binary systems exhibited slump flow diameters of less than 650mm, which falls outside the range recommended by EFNARC (32).

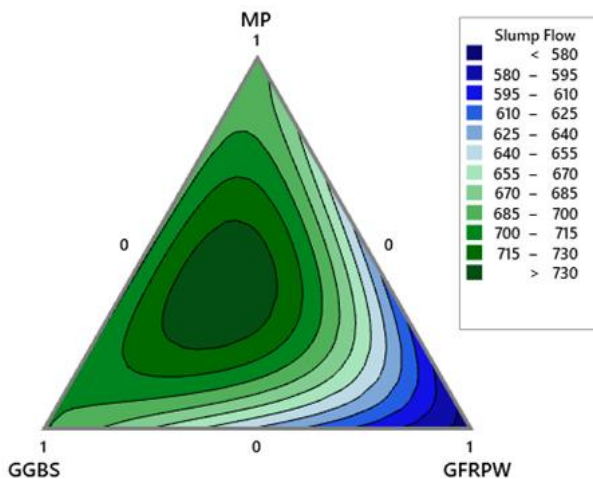


Fig. 10. Contour plot for Slump flow

For the MP-GGBS binary system, all SCC mixes produced slump flow values that met this recommendation. For the MP-GGBS binary system, increasing the MP content slightly increases the slump flow diameter. The optimum slump flow value is 742.69mm, corresponding to the mix proportions of 37% PM, 39% LA and 23% PV.

4.2. V-funnel

The V-funnel time allows the evaluation of the viscosity of SCC mixtures, where a high flow time reflects high viscosity and a low flow time indicates low viscosity. The results illustrated in Fig. 11 show that the addition of MP and GGBS in SCC mixtures leads to a decrease in the V-funnel time values. Several researchers have attributed the reduction in viscosity of MP-based cementitious systems to the thixotropic property of this mineral addition (2,33,34). Biricik et al. (34) stated that the incorporation of MP can diminish the thixotropy of cement-based materials due to its inert nature. The authors also reported that the smooth surface texture and rounded shape of the MP particles, as shown in Fig. 4(a), can improve the flow behaviour. Spherically shaped particles with a smooth surface create a ball-bearing effect, allowing the particles to slide easily over each other, thus reducing interparticle friction.

The GFRPW particles, characterised by their low specific gravity (Table 2), exhibit SCC mixtures with a high paste volume. The increase in cement paste volume helps to minimise the interaction and friction between the aggregate particles. Moreover, the addition of GFRPW causes an increase in the air content percentage, as shown in Fig. 12. According to Meko et al., the increase in air bubbles tends to decrease the friction between mortar and coarse aggregate (35). It is evident that the ability of MP and GFRPW particles to mitigate internal friction allows SCC mixtures to flow through the V-funnel more easily and quickly. Tittarelli et al. (18) also reported that the presence of surfactants at the surface of the polymer particles of GFRPW may allow for better dispersion, thus reducing the viscosity of cement paste.

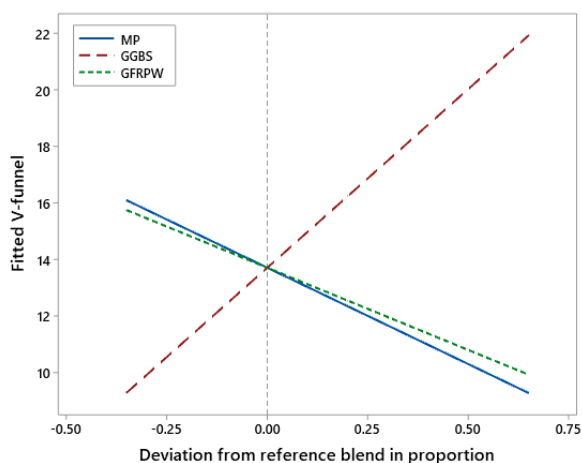


Fig. 11. Trace plot for V-funnel time

However, incorporating GGBS in the SCC mixes significantly increases the V-funnel time, as illustrated in Fig. 11. This behaviour can be explained by GGBS particles having a more angular shape and rough texture than MP particles, as shown in Fig. 4. Furthermore, the high specific gravity of GGBS particles (Table 2) contributes to decreasing the paste volume and, hence, increasing the internal friction of the SCC mixtures. Previous studies have also reported an increase in viscosity with the addition of GGBS (13,36,37).

The statistical model derived for V-funnel time is presented in Table 6. The model indicates that the V-funnel time is only influenced by the individual factors MP, GGBS, and GFRPW. Bouziani et al. (26) obtained comparable results when assessing the impact of three types of sand on the V-funnel flow time of SCC mixtures. The statistical model derived for V-funnel time was found to be independent of both ternary and binary interactions between the different sand types.

The effect of MP, GGBS, and GFRPW proportions on V-funnel time in binary and ternary systems is illustrated in Fig. 12. This figure indicates that the V-funnel time increases with increasing GGBS proportion in the GGBS-GFRPW, GGBS-MP, and MP-GFRPW-GGBS systems. Several studies have observed similar trends when incorporating GGBS in combination with different mineral admixtures (37). The figure also revealed that a GGBS proportion higher than 0.2 resulted in SCC mixtures with V-funnel times greater than 12 s, which is the upper limit recommended by EFNARC (32). On the other hand, the SCC mixtures in the GFRPW-MP binary system exhibited V-funnel time values ranging from 9 s to 10 s, meeting the EFNARC recommendations. The V-funnel time values ranged from a maximum of 22 s for 100% GGBS to a minimum of 9 s for 100% MP.

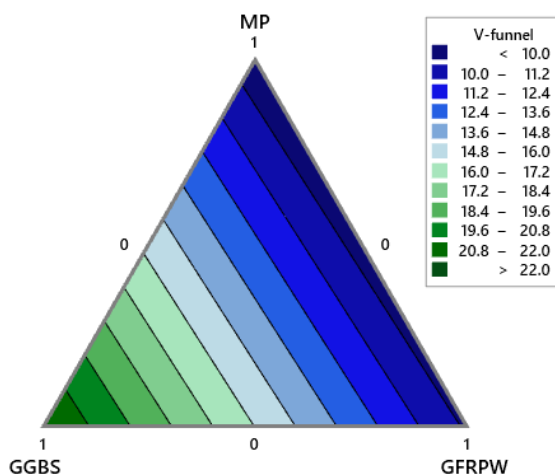


Fig. 12. Contour plot for V-funnel time

4.3. L-Box

The L-box ratio (H_2/H_1) assesses the filling and passing ability of the SCC mixtures. The trace plot of the L-box ratio (H_2/H_1), illustrated in Fig. 13, indicates that each of the additions MP, GGBS and GFRPW increases the L-box ratio at low proportions and then decreases it at high proportions. It is important to note that there is a proportional relationship between the L-box ratios and the slump flow values; the L-box ratio increases as the slump flow value increases, and vice versa. Nutan et al. (38) identified a good correlation between the L-box ratio and the yield stress of SCC mixtures, indicating that the L-box decreases as the yield stress increases. However, the GFRPW curve does not exhibit a significant drop in the L-box ratio, as observed in the slump flow. The reason can be attributed to the decrease in viscosity, illustrated in the V-funnel trace plot, which prevents a significant drop in the L-box ratio (39).

The statistical model of the L-box ratio indicates that the ternary combination MP*GGBS*GFRPW has the most significant influence, followed by the single factors MP, GGBS and GFRPW, respectively. The binary combinations GFRPW*GGBS and MP*GFRPW have a negative impact on the blocking ratio.

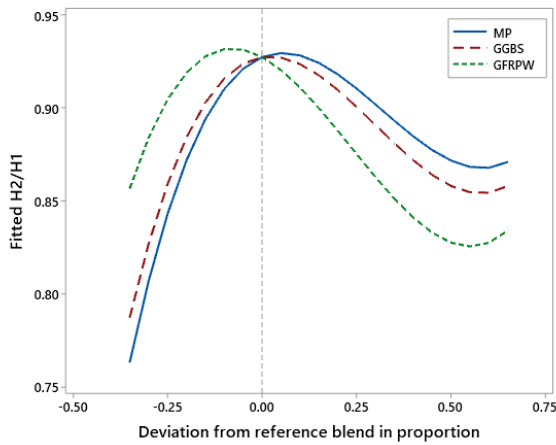


Fig. 13. Trace plot for L-Box ratio

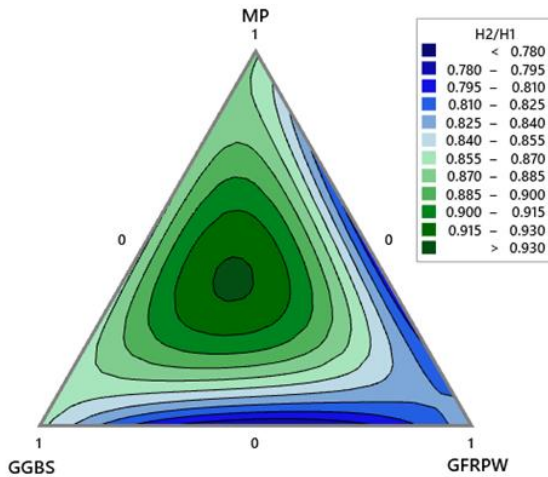


Fig. 14. Contour plot for L-Box ratio

From the contour plot of the L-Box ratio, illustrated in Fig. 14, it can be seen that all the blocking ratios in the MP-GGBS and MP-GFRPW binary systems fall within the range of 0.8 to 1 recommended by EFNARC. It can also be seen that the interaction between GGBS*GFRPW and MP*GFRPW exhibits an antagonistic effect on the blocking ratio. Mohammed et al. reported a similar effect between GGBS and FA, attributing it to the interlocking mechanism between the two types of particles (12). In the GFRPW-GGBS binary system, the L-box ratio falls below 0.8 when the GFRPW and GGBS proportions are between 0.3 and 0.7. According to EFNARC, a blocking ratio below 0.8 indicates a risk of mixture blockage (32). The SCC mix proportions of 39% PM, 36% LA and 25% PV yielded the optimum L-box ratio of 0.93.

4.4. Air Content

The air content measured using the pressure method provides insight into the air voids or bubble content in the fresh concrete. The majority of air bubbles are formed during the concrete mixing process and get entrapped between colliding fine aggregates (40). It can

be seen from the trace plot in Fig. 15 that the air content has a low sensitivity to the MP content. The slight negative slope in the corresponding curve reflects the adverse impact of MP on air content. Different parameters can contribute to the negative effect of MP addition on the air content. Zeng et al. reported that the low viscosity of fresh concrete facilitates the escape of air bubbles during mixing and placing (40). Puthipad et al. also found that particles of spherical shape may promote the coalescence of fine air bubbles into larger ones, making their collapse easier (41,42). In addition, the slight decrease in air content can reflect the minor effect of MP particles on improving the compactness of the mixes (43–45).

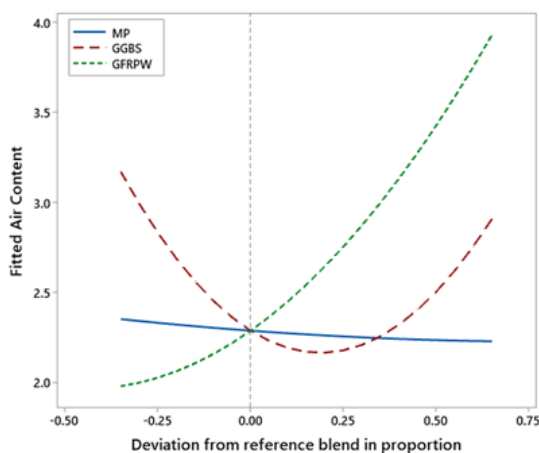


Fig. 15. Trace plot for Air content

Fig. 15 also shows that the addition of GGBS decreases the air content within a specific range and then increases it at high proportions. This observation can be related to the effect of GGBS particles on the mix's compactness. Initially, the GGBS particles probably fill the voids between the larger particles, making the mixes more compact and reducing the air content. Once the larger voids have been filled, the GGBS particles may start to create voids between each other, impairing the compactness of the mixes and increasing the air content (23,36). Moreover, the curve corresponding to GGBS demonstrates a good relationship between slump flow and air content of the SCC mixtures. Özcan et al. obtained a strong correlation between flow diameter and air content of non-air entrained concrete (46). It is well-known that low workability can generate a high amount of entrapped air due to improper placement of concrete mixes in the mould (46–48).

The air content trace plot (Fig. 15) illustrates the significant positive effect of GFRPW proportion on the air content. Most of the studies conducted on GFRPW incorporation in cementitious systems reported similar observations [24] (18,21,23,49). Coppola et al. found an anomalous air entrapment in fresh concrete, which was mitigated by a defoamer (21). Dehghan et al. attributed the increase in air content to the morphology of the GFRPW fibres, which promotes air entrapment (50). It is worth noting that the addition of GFRPW contributes to the loss of workability, as shown in Fig. 9, which may explain the increase in air entrapment in the SCC mixtures. Oliveira et al. also demonstrated that the poor hydrophilicity of the GFRPW particles prevents water absorption and facilitates the formation of air bubbles inside the mixtures (17). In a recent study, Zhou et al. (29) found that the addition of GFPW triggers apparent expansion in fresh mortar. The researchers identified that the amine curing agent of the resin and metallic oxides in the GFRPW react in an alkaline solution, resulting in gas production and fresh expansion. The expansion

generated during mixing could potentially explain the increase in the air content of the SCC mixtures (29,51).

The statistical model for air content (Table 6) indicates that the factors influencing air content are, in order of importance, GGBS*GFRPW, GFRPW, GGBS, MP*GGBS, and MP. The binary combination GGBS*GFRPW has the most significant impact on air content (-4.517). According to Ma et al., the pozzolanic reaction consumes the OH⁻ ions in cement paste, potentially mitigating the fresh-state expansion reaction and reducing gas generation (51). The combined effect of GGBS in improving the mixture compactness and reducing the expansion reaction with its pozzolanic reactivity might explain the notable negative impact of the GGBS*GFRPW combination on air content.

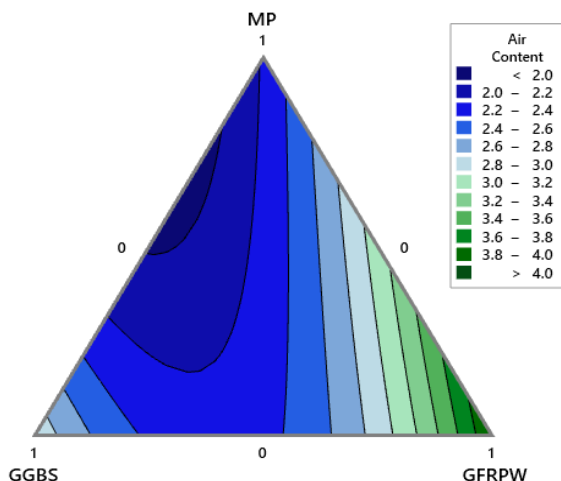


Fig. 16. Contour plot for Air content

The contour plot, illustrated in Fig. 16, shows that increasing the GFRPW content in the binary system MP-GFRPW elevates the air content in the SCC mixes. The binary combination of GGBS with MP and GFRPW produces an antagonistic effect on the air content. As depicted in Fig. 15, the addition of GGBS enhances the compactness of the SCC mixes within a specific range before decreasing it.

The highest air content percentage is 3.99%, recorded with 100% GFRPW. The highest air content percentage does not exceed the 5% allowed for SCC mixtures (51). It can be inferred that the addition of GFRPW contributes to the frost resistance of SCC (47). However, the lowest air content percentage is 1.93%, which was recorded with the combination of 65% MP and 35% GGBS.

4.5. Compressive Strength

Figs. 17 and 18 illustrate the trace plot of the compressive strength at 28 days (Rc28) and 90 days (Rc90), respectively. It can be seen from Fig.17 that the addition of GFRPW leads to a decrease in the 28-day compressive strength, as indicated by the downward trend of the corresponding curve. This decrease in 28-day strength can be attributed to the increase in the air content resulting from the addition of GFRPW, as illustrated in Fig. 15. Similar observations have been reported by several authors (21,49). Corinaldesi et al. successfully mitigated a 10% loss in compressive strength in SCC mixes containing GFRPW by adding a defoamer that decreased air entrapment (49). The reduction in compressive strength can also be related to the lower strength of the plastic particles compared to that of MP and GGBS particles. Tittarelli et al. reported that replacing calcareous filler with GFRPW

impairs the mechanical performance of SCC (24). Furthermore, the interaction zone between the GFRPW particles and the cement matrix may affect the concrete strength. The low hydrophilicity of GFRPW particles can lead to an accumulation of free water around their surface, which reduces the microstructure of their interaction zone with the cement matrix (52). Oliveira et al. attributed the loss of compressive strength to the weak bond between the polymer fraction of the GFRPW and the cement paste (17). Correia et al. also reported that the cylindrical shape of the GFRPW particles negatively impacts the interaction zone between the concrete's components (19). Upon examining the SEM images of GFRPW-based concrete, Zhao et al. observed that the GFRPW fibres were pulled out rather than broken, indicating a weak bond between the fibres and the matrix (53).

The negative effect of GFRPW on the 28-day compressive strength tends to decrease as the GFRPW proportion decreases. This tendency can be observed as the slope of the GFRPW curve decreases with the GFRPW content. A similar trend was observed by Correia et al., who reported a slight decrease in the 28-day compressive strength at low GFRPW incorporation rates(19).

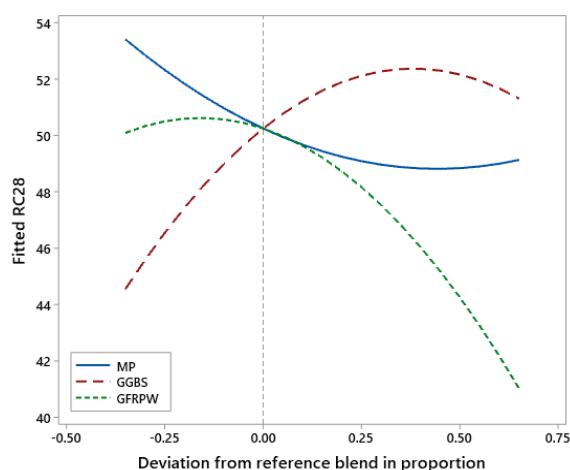


Fig. 17. Trace plot for RC28

It is worth noting that the influence of GFRPW on compressive strength changes at a later age. According to the GFRPW curve shown in Fig. 18, this waste material has a positive effect on the 90-day compressive strength in a specific range. The reason for the increase in the 90-day strength can be attributed to the presence of the chemical components SiO₂, CaO and Al₂O₃, which contribute to the hydration reaction and, thus, to the mechanical strength development (22). As the increase in mechanical strength was observed after 90 days of curing, it can be inferred that this behaviour is a result of the pozzolanic reactivity of GFRPW. Baturki et al. reported that GFRPW exhibits a high pozzolanic activity, which is mainly controlled by its silicate content and fineness (54).

However, beyond a certain threshold, the 90-day compressive strength decreases with increasing GFRPW content, as illustrated in Fig. 18. It is evident that a high proportion of GFRPW leads to the accumulation of more voids and poor interaction zones, which in turn weakens the concrete microstructure and reduces its strength. These results are in agreement with previous research (53,55).

The trace plot curve corresponding to MP, illustrated in Fig. 17 and 18, shows that MP has a negative impact on both 28-day and 90-day compressive strengths. It can be noticed that the slope of the MP curves steepens with age. These observations corroborate the earlier

suggestions that MP is an inert mineral addition with no pozzolanic activity (2,39,43). The inert nature of the MP prevents its involvement in the hydration process, limiting its ability to contribute to the development of the concrete's mechanical performance (56). In addition, excessive fines can weaken the bond between the aggregates and the cement matrix in the interfacial transition zone (ITZ), decreasing the strength of concrete. Meera and Gupta attributed the decrease in the concrete compressive and splitting strength after the incorporation of MP to the presence of a large amount of fines (57).

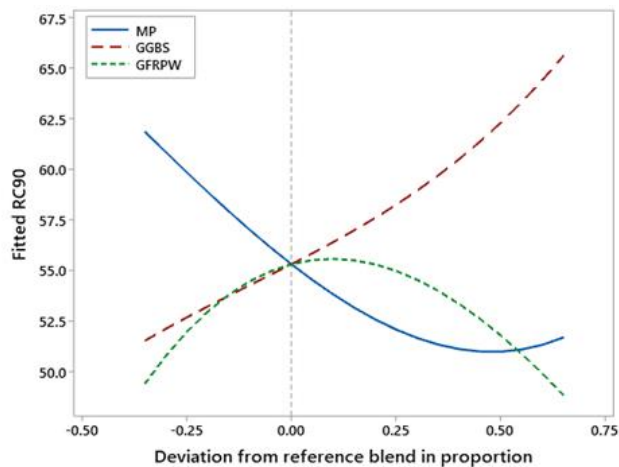


Fig. 18. Trace plot for Rc90

Fig. 17 and 18 also demonstrate that GGBS has a positive effect on compressive strengths at both ages. This influence becomes more pronounced at 90 days as the GGBS-related curve slope increases. According to Moula et al., GGBS particles act as nucleation sites for the formation and growth of hydrates, which enhances short-term strength and promotes the production of Portlandite for the long-term pozzolanic reaction (58). The trace plot curve related to GGBS, illustrated in Fig. 17, also shows a slight decrease in 28-day strength at high GGBS proportions. This result is consistent with that of air content. It is therefore possible to explain this loss of compressive strength by the increased porosity of the SCC mixtures. The loss in compressive strength was recovered after 90 days due to the long-term pozzolanic reactivity of GGBS. The long-term pozzolanic reaction of GGBS produces more hydrated calcium silicates (C-S-H) at a later age, which reduces the size of capillary pores, densifies the microstructure, and develops strength (11).

The statistical models for compressive strength at 28 days (Rc28) and 90 days (Rc90) are presented in Table 6. The factors influencing the compressive strength at 28 days are GGBS, MP, GFRPW and GGBS*GFRPW, respectively. The binary combination GGBS*GFRPW contributes to an increase in the 28-day compressive strength. It is evident that the significant influence of this parameter on reducing the air content (Table 6) enabled the development of compressive strength. Özcan et al. also reported an inverse relationship between 28-day compressive strength and air content (46), where the compressive strength increases as the air content of the fresh concrete decreases.

For the 90-day compressive strength, the influencing factors in order of importance are, GGBS, MP, GFRPW, MP*GGBS, MP*GFRPW*GGBS, GGBA*GFRPW, and MP*GFRPW. It is clear that the interaction terms MP*GGBS*GFRPW and MP*GFRPW promote the development of the 90-day compressive strength. Several researchers have reported that the use of pozzolanic additions in combination with MP improves the mechanical performance of concrete [9]. Choudhary et al. found that despite the negative effect of MP on mechanical

strength, the addition of FA improved the mechanical strength of SCC after 90 days of curing (2). However, the interaction term GGBS*MP has a negative influence on the 90-day compressive strength. Belaidi et al. obtained a reduction in compressive strength with the addition of PZ and MP (25). The authors stated that PZ incorporation causes a slow evolution of the compressive strength of MP-based concrete mixtures.

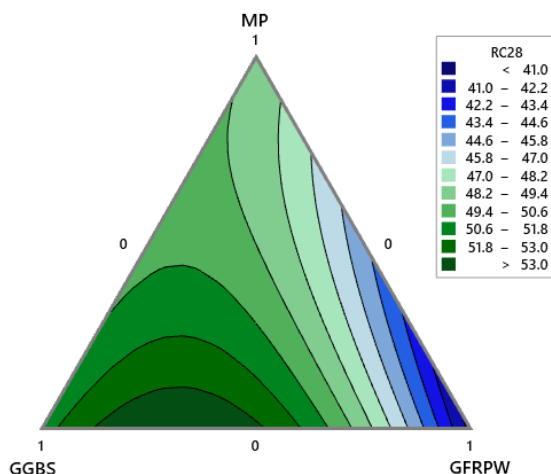


Fig. 19. Contour plot for RC28

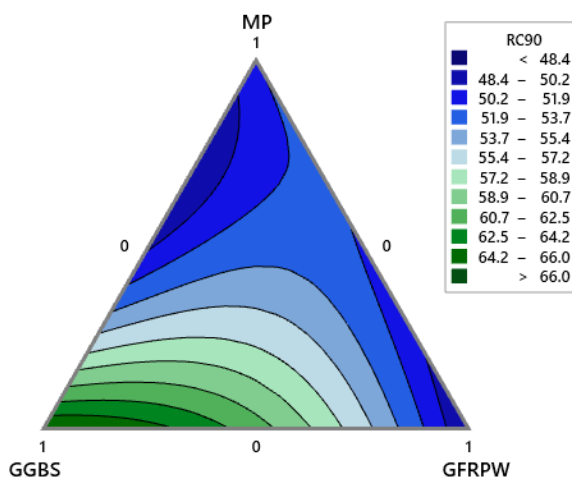


Fig. 20. Contour plot for RC90

The contour plot for compressive strength at 28 days is shown in Fig. 19. The figure shows that as the GFRPW content increases in the binary system MP-GFRPW, the compressive strength decreases. This behaviour can be attributed to the increase in air content in the SCC mixtures with increasing GFRPW proportion in the MP-GFRPW combination (Fig. 16). In the case of the GGBS-MP binary combination, the 28-day compressive strength improves with an increase in GGBS content due to the pozzolanic reactivity of this mineral addition, unlike the inert nature of MP. However, in the GGBS-GFRPW system, the increase in GGBS content increases the compressive strength to a maximum value of 54.19MPa, corresponding to the combination of 32% GFRPW with 68% GGBS, and then decreases it. These results are consistent with those for air content in the GGBS-GFRPW binary system,

where GGBS reduces the air content of SCC mixes before subsequently increasing it. The minimum 28-day compressive strength value is 40.60 MPa, corresponding to the 100% GFRPW proportion.

Regarding the 90-day compressive strength, it can be seen from Fig. 20 that the effect of the mineral additions in both the binary and ternary systems change with time. Increasing the GGBS proportion in the GGBS-GFRPW binary system develops the compressive strength to a maximum value of 66.02 MPa, corresponding to the mix proportion of 100% GGBS, and shows no decreasing effect. This suggests that the long-term pozzolanic reactivity of GGBS contributes to the refinement of the capillary pores that negatively affect the 28-day strength. The interaction in the MP-GGBS binary system causes an antagonistic effect on the 90-day compressive strength. This behaviour is not consistent with the air content results, where the binary combination MP-GGBS shows the minimum air content percentage. This implies that the air content of the fresh concrete is not the only parameter that can explain the development of concrete strength. As for the 28-day compressive strength, the minimum 90-day compressive strength corresponds to the proportion of 100% GFRPW and is equal to 48.44 MPa.

5. Conclusions

The mixture design modeling approach was adopted in this study to evaluate the impact of combining three local waste materials, namely MP, GGBS, and GFRPW, as mineral additions on the performance of SCC. Based on the results obtained, the following conclusions can be drawn:

- MP, GGBS, and GFRPW exhibited a similar effect on slump flow, with the slump flow value increasing within a specific range and then decreasing. When the proportion of GFRPW in the GFRPW-based binary systems exceeded 0.5, the SCC mixes produced slump flow values below the lower limit of 650 mm recommended by EFNARC. The interaction between the three components $MP*GGBS*GFRPW$ promoted an increase in slump flow, reaching a maximum value of 742.69 mm at proportions of 37% MP, 39% GGBS, and 23% GFRPW.
- GFRPW and MP had a similar decreasing effect on the V-funnel time, while GGBS demonstrated an increasing effect. When the proportion of GGBS exceeded 0.2 in the GGBS-based systems, the SCC mixtures resulted in V-funnel time values above 12s, which does not meet the EFNARC recommendations.
- MP, GFRPW, and GGBS had a similar effect on the blocking ratio, with the L-box ratio increasing within a specific range before decreasing. The ternary interaction $MP*GFRPW*GGBS$ contributed to an increase in the L-box ratio, reaching a maximum value of 0.93 at proportions of 39% MP, 36% GGBS, and 25% GFRPW. However, the binary interactions $GFRPW*GGBS$ and $GFRPW*MP$ caused a decrease in the blocking ratio. In the GGBS-GFRPW binary system, when the proportion of GFRPW was between 0.3 and 0.7, the SCC mixtures had L-box ratios below the EFNARC recommended lower limit of 0.8.
- GFRPW had a significant effect on increasing the air content of fresh SCC mixtures, with the maximum value of 3.99% recorded at a mixture proportion of 100% GFRPW. The interaction in the binary systems $GFRPW*MP$ and $GFRPW*GGBS$ resulted in a decrease in the air content. MP had a minimal impact on the air content, while GGBS initially decreased the air content within a specific range before increasing it.
- Increasing the amount of GRPW resulted in a decrease in compressive strength at 28 and 90 days, reaching a minimum value of 40.60 MPa and 48.44 MPa, respectively, for 100% GRPW. The interaction between GGBS and GFRPW gave a maximum 28-day compressive strength of 54.19 MPa for a mix containing 68%

GGBS and 32% GFRPW. The maximum 90-day compressive strength was 66.02 MPa for 100% GGBS.

References

- [1] De Schutter G, editor. Self-compacting concrete. Dunbeath: Whittles Publ. [u.a.]; 2008. 296 p.
- [2] Choudhary R, Gupta R, Nagar R. Impact on fresh, mechanical, and microstructural properties of high strength self-compacting concrete by marble cutting slurry waste, fly ash, and silica fume. *Constr Build Mater.* 2020;239:117888. <https://doi.org/10.1016/j.conbuildmat.2019.117888>
- [3] Iqbal Q, Musarat MA, Ullah N, Alaloul WS, Rabbani MBA, Al Madhoun W, et al. Marble dust effect on the air quality: An environmental assessment approach. *Sustainability.* 2022;14(7):3831. <https://doi.org/10.3390/su14073831>
- [4] Sufian M, Ullah S, Ostrowski KA, Ahmad A, Zia A, Śliwa-Wieczorek K, et al. An experimental and empirical study on the use of waste marble powder in construction material. *Materials.* 2021;14(14):3829. <https://doi.org/10.3390/ma14143829>
- [5] Singh M, Choudhary K, Srivastava A, Sangwan KS, Bhunia D. A study on environmental and economic impacts of using waste marble powder in concrete. *J Build Eng.* 2017;13:87-95. <https://doi.org/10.1016/j.jobe.2017.07.009>
- [6] Butt IM, Mustafa T, Rauf S, Razzaq A, Anwer J. Pulmonary function parameters among marble industry workers in Lahore, Pakistan. *F1000Research* [Internet]. 2021 [cited 2024 Mar 23];10. <https://doi.org/10.12688/f1000research.52749.1>
- [7] Meera M, Dash AK, Gupta S. Rheological and strength properties of self-compacting concrete incorporating marble and granite powders. *Mater Today Proc.* 2020;32:1005-13. <https://doi.org/10.1016/j.matpr.2020.08.531>
- [8] Sadek DM, El-Attar MM, Ali HA. Reusing of marble and granite powders in self-compacting concrete for sustainable development. *J Clean Prod.* 2016;121:19-32. <https://doi.org/10.1016/j.jclepro.2016.02.044>
- [9] Mahmood MS, Elahi A, Zaid O, Alashker Y, Šerbănoiu AA, Grădinaru CM, et al. Enhancing compressive strength prediction in self-compacting concrete using machine learning and deep learning techniques with incorporation of rice husk ash and marble powder. *Case Stud Constr Mater.* 2023;19:e02557. <https://doi.org/10.1016/j.cscm.2023.e02557>
- [10] Bayat H, Banar R, Nikravan M, Farnood P, Ramezaniyanpour AM, Kashani A. Durability, mechanical, workability, and environmental assessment of self-consolidating concrete containing blast furnace slag and natural zeolite. *J Build Eng.* 2024;108737. <https://doi.org/10.1016/j.jobe.2024.108737>
- [11] Sara B, Mhamed A, Otmame B, Karim E. Elaboration of a Self-Compacting mortar based on concrete demolition waste incorporating blast furnace slag. *Constr Build Mater.* 2023;366:130165. <https://doi.org/10.1016/j.conbuildmat.2022.130165>
- [12] Mohammed AM, Asaad DS, Al-Hadithi AI. Experimental and statistical evaluation of rheological properties of self-compacting concrete containing fly ash and ground granulated blast furnace slag. *J King Saud Univ-Eng Sci.* 2022;34(6):388-97. <https://doi.org/10.1016/j.jksues.2020.12.005>
- [13] Ofuyatan OM, Adeniyi AG, Ijie D, Ighalo JO, Oluwafemi J. Development of high-performance self compacting concrete using eggshell powder and blast furnace slag as partial cement replacement. *Constr Build Mater.* 2020;256:119403 <https://doi.org/10.1016/j.conbuildmat.2020.119403>
- [14] Hadigheh SA, Wei Y. Recycling of glass fibre reinforced polymer (GFRP) composite wastes in concrete: A critical review and cost benefit analysis. In: *Structures* [Internet]. Elsevier; 2023 [cited 2024 Jan 27]. p. 1540-56. <https://doi.org/10.1016/j.istruc.2023.05.018>

- [15] Gonçalves RM, Martinho A, Oliveira JP. Recycling of reinforced glass fibers waste: Current status. *Materials*. 2022;15(4):1596. <https://doi.org/10.3390/ma15041596>
- [16] Oliveira PS, Antunes MLP, da Cruz NC, Rangel EC, de Azevedo ARG, Durrant SF. Use of waste collected from wind turbine blade production as an eco-friendly ingredient in mortars for civil construction. *J Clean Prod*. 2020;274:122948. <https://doi.org/10.1016/j.jclepro.2020.122948>
- [17] Tittarelli F, Shah SP. Effect of low dosages of waste GRP dust on fresh and hardened properties of mortars: Part 1. *Constr Build Mater*. 2013;47:1532-8. <https://doi.org/10.1016/j.conbuildmat.2013.06.043>
- [18] Correia JR, Almeida NM, Figueira JR. Recycling of FRP composites: reusing fine GFRP waste in concrete mixtures. *J Clean Prod*. 2011;19(15):1745-53. <https://doi.org/10.1016/j.jclepro.2011.05.018>
- [19] Asokan P, Osmani M, Price AD. Assessing the recycling potential of glass fibre reinforced plastic waste in concrete and cement composites. *J Clean Prod*. 2009;17(9):821-9. <https://doi.org/10.1016/j.jclepro.2008.12.004>
- [20] Coppola L, Cadoni E, Forni D, Buoso A. Mechanical characterization of cement composites reinforced with fiberglass, carbon nanotubes or glass reinforced plastic (GRP) at high strain rates. *Appl Mech Mater*. 2011;82:190-5. <https://doi.org/10.4028/www.scientific.net/AMM.82.190>
- [21] Asokan P, Osmani M, Price AD. Improvement of the mechanical properties of glass fibre reinforced plastic waste powder filled concrete. *Constr Build Mater*. 2010;24(4):448-60. <https://doi.org/10.1016/j.conbuildmat.2009.10.017>
- [22] Farinha CB, de Brito J, Veiga R. Assessment of glass fibre reinforced polymer waste reuse as filler in mortars. *J Clean Prod*. 2019;210:1579-94. <https://doi.org/10.1016/j.jclepro.2018.11.080>
- [23] Tittarelli F, Moriconi G. Use of GRP industrial by-products in cement based composites. *Cem Concr Compos*. 2010;32(3):219-25. <https://doi.org/10.1016/j.cemconcomp.2009.11.005>
- [24] Belaidi ASE, Azzouz L, Kadri E, Kenai S. Effect of natural pozzolana and marble powder on the properties of self-compacting concrete. *Constr Build Mater*. 2012;31:251-7. <https://doi.org/10.1016/j.conbuildmat.2011.12.109>
- [25] Bouziani T. Assessment of fresh properties and compressive strength of self-compacting concrete made with different sand types by mixture design modelling approach. *Constr Build Mater*. 2013;49:308-14. <https://doi.org/10.1016/j.conbuildmat.2013.08.039>
- [26] Mendes BC, Pedroti LG, Vieira CMF, de Carvalho JMF, Ribeiro JCL, de Souza CMM. Application of mixture design of experiments to the development of alkali-activated composites based on chamotte and waste glass. *Constr Build Mater*. 2023;379:131139. <https://doi.org/10.1016/j.conbuildmat.2023.131139>
- [27] Chen C, Li X, Chen X, Chai J, Tian H. Development of cemented paste backfill based on the addition of three mineral additions using the mixture design modeling approach. *Constr Build Mater*. 2019;229:116919. <https://doi.org/10.1016/j.conbuildmat.2019.116919>
- [28] Zhou B, Zhang M, Ma G. Multi-scale experimental study on the effect of crushed GFRP powder and dust on physical-mechanical properties of cement mortar. *J Build Eng*. 2022;57:104853. <https://doi.org/10.1016/j.jobbe.2022.104853>
- [29] Chen CH, Huang R, Wu JK, Yang CC. Waste E-glass particles used in cementitious mixtures. *Cem Concr Res*. 2006;36(3):449-56. <https://doi.org/10.1016/j.cemconres.2005.12.010>
- [30] Dada H, Belaidi ASE, Soualhi H, Kadri EH, Benabed B. Influence of temperature on the rheological behaviour of eco-mortar with binary and ternary cementitious blends of natural pozzolana and marble powder. *Powder Technol*. 2021;384:223-35. <https://doi.org/10.1016/j.powtec.2021.02.019>

- [31] EFNARC F. Specification and guidelines for self-compacting concrete. Eur Fed Spec Constr Chem Concr Syst. 2002;
- [32] Prakash B, Saravanan TJ, Kabeer KSA, Bisht K. Exploring the potential of waste marble powder as a sustainable substitute to cement in cement-based composites: A review. Constr Build Mater. 2023;401:132887.
- [33] Biricik Ö, Aytekin B, Mardani A. Effect of waste binder material usage rate on thixotropic behaviour of cementitious systems. Constr Build Mater. 2023;403:133197. <https://doi.org/10.1016/j.conbuildmat.2023.133197>
- [34] Meko B, Ighalo JO, Ofuyatan OM. Enhancement of self-compactability of fresh self-compacting concrete: A review. Clean Mater. 2021;1:100019. <https://doi.org/10.1016/j.clema.2021.100019>
- [35] Revilla-Cuesta V, Skaf M, Santamaría A, Hernández-Bagaces JJ, Ortega-López V. Temporal flowability evolution of slag-based self-compacting concrete with recycled concrete aggregate. J Clean Prod. 2021;299:126890. <https://doi.org/10.1016/j.jclepro.2021.126890>
- [36] Khodair Y, Bommareddy B. Self-consolidating concrete using recycled concrete aggregate and high volume of fly ash, and slag. Constr Build Mater. 2017;153:307-16. <https://doi.org/10.1016/j.conbuildmat.2017.07.063>
- [37] Nguyen TLH, Roussel N, Coussot P. Correlation between L-box test and rheological parameters of a homogeneous yield stress fluid. Cem Concr Res. 2006;36(10):1789-96. <https://doi.org/10.1016/j.cemconres.2006.05.001>
- [38] Uysal M, Yilmaz K. Effect of mineral admixtures on properties of self-compacting concrete. Cem Concr Compos. 2011;33(7):771-6. <https://doi.org/10.1016/j.cemconcomp.2011.04.005>
- [39] Zeng X, Lan X, Zhu H, Liu H, Umar HA, Xie Y, et al. A review on bubble stability in fresh concrete: Mechanisms and main factors. Materials. 2020;13(8):1820. <https://doi.org/10.3390/ma13081820>
- [40] Wang Y, Lu H, Xiao R, Hu W, Huang B. Experimental Study on the Stability and Distribution of Air Voids in Fresh Fly Ash Concrete. Materials. 2022;15(23):8332. <https://doi.org/10.3390/ma15238332>
- [41] Puthipad N, Ouchi M, Attachaiyawuth A. Effects of fly ash, mixing procedure and type of air-entraining agent on coalescence of entrained air bubbles in mortar of self-compacting concrete at fresh state. Constr Build Mater. 2018;180:437-44. <https://doi.org/10.1016/j.conbuildmat.2018.04.138>
- [42] Alyousef R, Benjeddou O, Soussi C, Khadimallah MA, Mustafa Mohamed A. Effects of incorporation of marble powder obtained by recycling waste sludge and limestone powder on rheology, compressive strength, and durability of self-compacting concrete. Adv Mater Sci Eng [Internet]. 2019 [cited 2024 Jan 31];2019. <https://doi.org/10.1155/2019/4609353>
- [43] Ahmad J, Zhou Z, Deifalla AF. Self-Compacting Concrete with Partially Substitution of Waste Marble: A Review. Int J Concr Struct Mater. 2023 Apr 17;17(1):25. <https://doi.org/10.1186/s40069-023-00585-5>
- [44] Danish A, Mosaberpanah MA, Salim MU, Fediuk R, Rashid MF, Waqas RM. Reusing marble and granite dust as cement replacement in cementitious composites: A review on sustainability benefits and critical challenges. J Build Eng. 2021;44:102600. <https://doi.org/10.1016/j.jobe.2021.102600>
- [45] Özcan F, Koç ME. Influence of ground pumice on compressive strength and air content of both non-air and air entrained concrete in fresh and hardened state. Constr Build Mater. 2018;187:382-93. <https://doi.org/10.1016/j.conbuildmat.2018.07.183>

- [46] Topcu IB, Bilir T, Uygunoğlu T. Effect of waste marble dust content as filler on properties of self-compacting concrete. *Constr Build Mater.* 2009;23(5):1947-53. <https://doi.org/10.1016/j.conbuildmat.2008.09.007>
- [47] Ahmad J, Zhou Z. Mechanical performance of waste marble based self compacting concrete reinforced with steel fiber (Part I). *J Build Eng.* 2023;78:107574. <https://doi.org/10.1016/j.jobbe.2023.107574>
- [48] Corinaldesi V. Influence of lightweight aggregates and GRP by-product powders on the properties of self-compacting concretes. *Adv Mater Res.* 2012;548:215-20. <https://doi.org/10.4028/www.scientific.net/AMR.548.215>
- [49] Dehghan A, Peterson K, Shvarzman A. Recycled glass fiber reinforced polymer additions to Portland cement concrete. *Constr Build Mater.* 2017;146:238-50. <https://doi.org/10.1016/j.conbuildmat.2017.04.011>
- [50] Ma G, Zhou B, Zhang M, Sanjayan J. Understanding and eliminating of expansion caused by recycled glass fiber reinforced plastic powder in concrete. *Constr Build Mater.* 2022;347:128542. <https://doi.org/10.1016/j.conbuildmat.2022.128542>
- [51] Aravecchia N, Bañuls-Ciscar J, Caverzan A, Ceccone G, Cuenca E, Ferrara L, et al. On the feasibility of using Polyester (PE) waste particles from metal coating industry as a secondary raw materials in concrete. *Clean Mater.* 2023;100193. <https://doi.org/10.1016/j.clema.2023.100193>
- [52] Zhao T, Lv Y, Chen J, Song P, Sun M, Zhang X, et al. Effect of Glass Fiber-Reinforced Plastic Waste on the Mechanical Properties of Concrete and Evaluation of Its Feasibility for Reuse in Concrete Applications. *Materials.* 2023;16(20):6772. <https://doi.org/10.3390/ma16206772>
- [53] Baturkin D, Hisseine OA, Masmoudi R, Tagnit-Hamou A, Massicotte L. Valorization of recycled FRP materials from wind turbine blades in concrete. *Resour Conserv Recycl.* 2021;174:105807. <https://doi.org/10.1016/j.resconrec.2021.105807>
- [54] Aziz F, Tan AR, Bakar NB, Nasir NAM. Properties of concrete with glass fibre reinforced polymer waste as partial replacement of fine aggregate. In: *Journal of Physics: Conference Series* [Internet]. IOP Publishing; 2023; 012015. <https://doi.org/10.1088/1742-6596/2521/1/012015>
- [55] Meera M, Gupta S. Performance evaluation of marble powder and fly ash concrete for non-structural applications. *J Build Eng.* 2024;84:108499. <https://doi.org/10.1016/j.jobbe.2024.108499>
- [56] Essam A, Mostafa SA, Khan M, Tahwia AM. Modified particle packing approach for optimizing waste marble powder as a cement substitute in high-performance concrete. *Constr Build Mater.* 2023;409:133845. <https://doi.org/10.1016/j.conbuildmat.2023.133845>
- [57] Moula S, Fraj AB, Wattez T, Bouasker M, Ali NBH. Mechanical properties, carbon footprint and cost of ultra-high performance concrete containing ground granulated blast furnace slag. *J Build Eng.* 2023;79:107796. <https://doi.org/10.1016/j.jobbe.2023.107796>